ACS OMEGA

Open Access

http://pubs.acs.org/journal/acsodf

Article

High Recovery of Ceramic Membrane Cleaning Remediation by Ozone Nanobubble Technology

Ande F. Rafryanto, Zakia D. P. Ramadina, Syarifa Nur'aini, Bagas H. Arrosyid, Akmal Zulfi, Nurul T. Rochman, Alfian Noviyanto,* and Arramel*

Cite This: *ACS Omega* 2024, 9, 11484−11493

Read Online

ACCESS | Metrics & More | Article Recommendations | Supporting Information

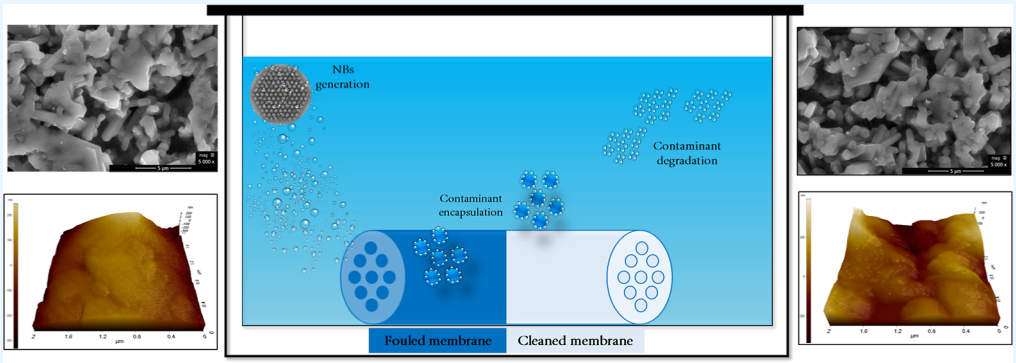

ABSTRACT: The persistent issue of ceramic membrane fouling poses significant challenges to its widespread implementation. To address this concern, ozone nanobubbles (ozone-NBs) have garnered attention due to their remarkable mass transfer efficiency. In this investigation, we present a novel ozone-NB generator system to effectively clean a fouled ceramic membrane that is typically employed in the dye industry. The surface characteristics of the ceramic membrane underwent significant alterations, manifesting incremental changes in surface roughness and foulant accumulation reduction, as evidenced in atomic force microscopy, scanning electron microscopy, X-ray fluorescence, and energy-dispersive spectroscopy. Remarkably, the sequential 4 h cleaning process demonstrates an effective outcome leading to an almost 2-fold enhancement in the membrane flux. The initial fouled state of 608 L/h/m^2 increased to 1050 L/h/m^2 in the 4 h state with a recovery of 50%. We propose such membrane performance improvement governed by the ozone-NBs with a size distribution of 213.2 nm and a zeta potential value of −20.26 ± 0.13 mV, respectively. This effort showcases a substantial innovative and sustainable technology approach toward proficient foulant removal in water treatment applications.

1. INTRODUCTION

Membrane filtration is a highly effective and versatile pressure-driven separation technique utilized for particles' mechanical and chemical sieving.[1,2] Among the commonly employed membrane materials, ceramic and polymeric membranes stand out as prominent options. Ceramic membranes, in particular, offer several distinct advantages over their polymeric counterparts. Ceramic membranes display exceptional mechanical strength, durability, and resistance to harsh chemical cleaning processes.[3] Moreover, ceramic membranes are well-suited for high-temperature environments and effectively handle slurries containing abrasive suspended materials. Their inherent resistance to biological deterioration further enhances their appeal in various industries. These membranes have gained widespread usage in these sectors, enabling efficient solid−liquid separation processes.[3−6]

Unfortunately, membrane fouling is a persistent challenge encountered in the operation of membranes, particularly in water and wastewater treatment. This issue has garnered significant attention due to the widespread adoption of membrane technology in these domains.[7] The fouling phenomenon mostly occurs as a result of the precipitation and deposition of undesired molecules or particles onto the membrane surfaces and pores.[8] It is worth noting that the fouling not only reduces the flow of the stream passing through the membrane but also has a substantial impact on the membrane's selectivity due to pore blockage (size exclusion), changes in surface chemistry, and the adsorption of foulants.[2,9−12]

Received: October 24, 2023
Revised: February 11, 2024
Accepted: February 13, 2024
Published: February 28, 2024

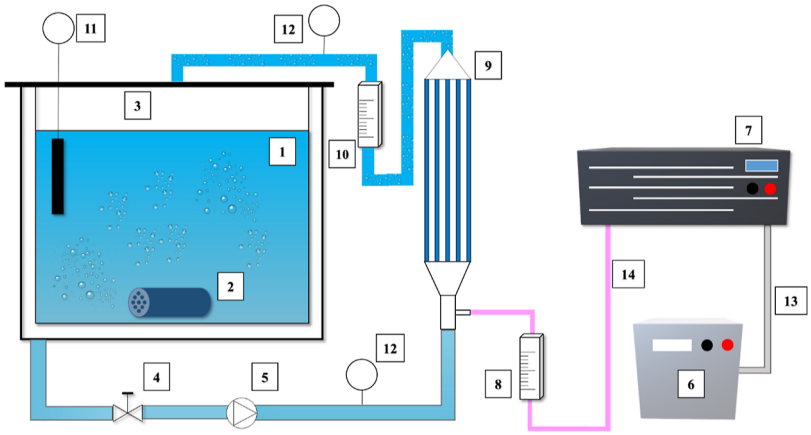

Figure 1. Schematic diagram of experiment apparatus: (1) water, (2) ceramic membrane, (3) tank, (4) valve, (5) distribution pump, (6) oxygen concentrator, (7) ozone generator, (8) gas flowmeter, (9) NB generator, (10) rotameter, (11) temperature indicator, (12) pressure indicator, (13) oxygen, and (14) ozone.

In recent years, several technologies have been proposed to address fouling. For example, in situ and ex situ methods consist of backwashing, air/gas sparing, scouring, and chemical cleaning. However, it is important to note that these methods often suffer non-negligible drawbacks such as being energy-intensive and potentially harmful to the membrane surface.[7,13] For instance, in backwashing, the elevated pressure and flow rate could potentially harm the membrane's surface and its structural integrity.[3,13] In addition, the nature of foulants, such as abrasives, is potent to harm the membrane during backwashing. Therefore, sustainable and effective fouling mitigation strategies in membrane technology development are highly desired to counter such issues.

Researchers are currently focusing on the development of microbubble (MB) and nanobubble (NB) technologies for membrane cleaning.[3,14] NBs specifically have higher mass transfer and bursting energy compared to MBs. Temesgen et al. proposed that NBs are bubbles with less than 1 μm in size, while MBs have slightly larger sizes in the range of 10−100 μm.[15] Several reports have discussed the utilization of air as a gas phase in NBs, considering the oxygen content, as reported by Dayarathne et al. and Ghadimkhani et al. Dayarathne et al. demonstrated that water containing air-MBs and air-NBs could disrupt the concentration polarization layer that forms on reverse osmosis membranes.[14] Ghadimkhani et al. investigated the cleaning of ceramic membranes using air-NBs and observed its effectiveness in removing synthetic fouling caused by NaCl and $MgCl_2$.[3] However, air is not categorized as a strong oxidant, and the generation of reactive oxygen species (ROS) that plays a crucial role in the degradation could be achieved only through water pyrolysis.[16] Therefore, providing an efficient and effective potent oxidant in the form of NBs is required.

Ozone is a promising oxidant in NB systems considering the high reduction potential. Additionally, in the ozone-NB system, ROS could potentially be generated not only by water pyrolysis but also by ozonation reaction through an indirect way.[16−18] NBs act as a physical barrier, effectively encapsulating the contaminating layers on its surface.[19−22] When contamination-encapsulated, the oxidant would oxidize it. Compared to larger bubbles, ozone-based NBs produced by NB generators exhibit a longer lifetime in the water column.[23] When dissolved ozone interacts with impurities, the treated water maintains the saturated ozone concentration, as highlighted by Meegoda and Batagoda[24] As a result, NBs retain their physical characteristics within the water column for several months under normal pressure conditions. Hutagalung et al. investigated the combined use of ozone-NBs and advanced oxidation processes to remove the dye effluent. The findings indicated that ozone-NBs exhibited a significantly higher capability, removing 60% of chemical oxygen demand compared to macro bubbles with only 40% removal efficiency.[17]

Tian et al. reported that continuous air bubbling was effective in reducing fouling. Additionally, the size of the air bubbles was found to influence membrane fouling.[25] However, the specific effects of these parameters in ozone-NBs on the cleaning process in membrane filtration have not been extensively explored. To address this research gap, this study focuses on examining the cleaning process using an ozone-NB system. The contaminated membrane used in the experiment was obtained from a dye-filtering company. The primary objective of this research is to gain insights into the underlying mechanisms of the physical interactions between ozone-NBs and ceramic membranes as well as the cleaning processes. By investigating these aspects, the study aims to understand better the utilization of ozone-NBs toward effective cleaning in membrane filtration systems.

2. MATERIALS AND METHODS

2.1. Experimental Setup. Our system consists of three sequential processes: NB generation, cleaning, and circulation. The schematic of the cleaning system is illustrated in Figure 1. It is readily apparent that the fouled ceramic membrane is positioned within the enclosed water tank with a volume of 3 m^3. The membrane is classified as ultrafilters (UFs) equipped with a pore size of 0.05 μm. Additionally, the diameter of this membrane is around 41 mm with 19 pieces of 6 mm channels. The material composition of the membrane filter layer is TiO_2, while the supporting shell is composed of Al_2O_3. Table 1 presents the detailed information on ceramic membranes.

The fouled membrane employed in this study was obtained from a company called Perusahaan Umum Percetakan Uang Republik Indonesia, which initially employed the membrane to filter dye solution. Thus, in this study, the experimental fouling process of ceramic membranes was not a focus. The flux of the fouled membrane was measured at 608 L/h/m^2 by using the

https://doi.org/10.1021/acsomega.3c08379
ACS Omega 2024, 9, 11484−11493

Table 1. Ceramic Membrane Specification

manufacturer	WTG Water Treatment GmbH
membrane type	tubular
material membrane supporting shell	α-Al_2O_3
material membrane filter layer	UF: TiO_2
pore size	50 nm
portable water flux	1500 L/h/m^2 (working pressure 3 bar)
number of channels	19
channel diameter	6 mm
pH working area of operations	0 to 14

flux test instrument for the cross-flow membrane[26] depicted in Figure 2. A distribution pump facilitated the circulation of water throughout the system. The water stream was then directed through a NB generator and injected with ozone. The ozone gas was generated from oxygen as the source using an ozone generator, employing the corona discharge method to ensure sufficient ozone production. We used ∼30 g/L ozone with concentrated oxygen produced from a concentrator (Yuwell 8F-3AW) to achieve a purity level exceeding 90%. The NB generator employed in this study shares conceptual similarities with the orifice plate principle outlined in the previous research.[17,27] The plate dimension is 50.8 mm in diameter and within one unit comprising 15 sets of plates. The NB generator consists of 114 honeycomb-shaped holes with a diameter of 2.35 mm and a spacing of 1 mm.

The inlet water containing NBs is directed into the tank housing the fouled membrane to facilitate fouling removal. Subsequently, water is continuously circulated through the system using a distribution pump. The duration of this process in our study varied from 1, 2, 3, and 4 h, respectively. It is worth mentioning that NB technology operates based on the occurrence of cavitation, which results from a significant decrease in pressure within the flow. Our previous research has demonstrated that our system achieved a cavitation number (Cv) of around 0.909.[17] According to Saharan et al., the cavitation phenomenon typically occurs when $Cv \leq 1$.[28−30]

2.2. Characterizations. The morphologies and structures of the ceramic membranes were characterized and analyzed using surface-based techniques such as atomic force microscopy (AFM, Park NX10) and field-emission scanning electron microscopy (FE-SEM, Thermo Scientific Quanta 650). The percentage of each element present on the surface of the ceramic membrane was confirmed using energy-dispersive spectroscopy (EDS) analysis equipped with the FE-SEM setup. The porosity of the membrane surface was determined through a two-dimensional calculation on the scanning electron microscopy (SEM) image, following the methodology in previous studies.[31,32] The elemental component of the dye, which served as the source of the foulant in this experiment, was determined using X-ray fluorescence (XRF) analysis conducted on a Rigaku NEX OC+EZ series instrument (serial number QC1520) operating in the range 3000−20,000 keV. The chemical bonds in the foulants were analyzed by Fourier transform infrared spectroscopy (FTIR, Thermo Scientific Nicolet iS10).

To analyze the size distribution and zeta potential of ozone-generated NB in water, a particle size analyzer (Zetasizer Pro Blue, Malvern) was employed based on the dynamic light scattering method. This instrument is capable of determining bubble sizes in the range of 0.3 nm−10 μm.

2.3. Membrane Flux Test. The cleaning performance was assessed by quantifying the outgoing membrane flux across the system, which was evaluated by using a comprehensive setup consisting of a hydraulic compressor, valves, a membrane holder, a pressure regulator, and an analytical balance. The membrane flux system is depicted in Figure 2. The applied pressure of the membrane flux was maintained at approximately 3 bar, simulating the operational conditions under which these membranes are employed. The membrane flux, also called water flux, is precisely defined as the volume of water that passes through the tested membrane per unit of time and area.[33] In addition, several other transport features such as rejection or retention and selectivity parameters could be useful to further characterize fouling formation. However, our focus in this investigation specifically related to the emphasis on water flux due to its feasibility within the available infrastructure. This flux value can provide insights into the energy requirements of the filtration process. This flux value can provide insights into the energy requirements of the filtration process. An ideal filter should exhibit a high water flux, which signifies a lower energy consumption during filtration. The membrane flux (J) can be calculated using the

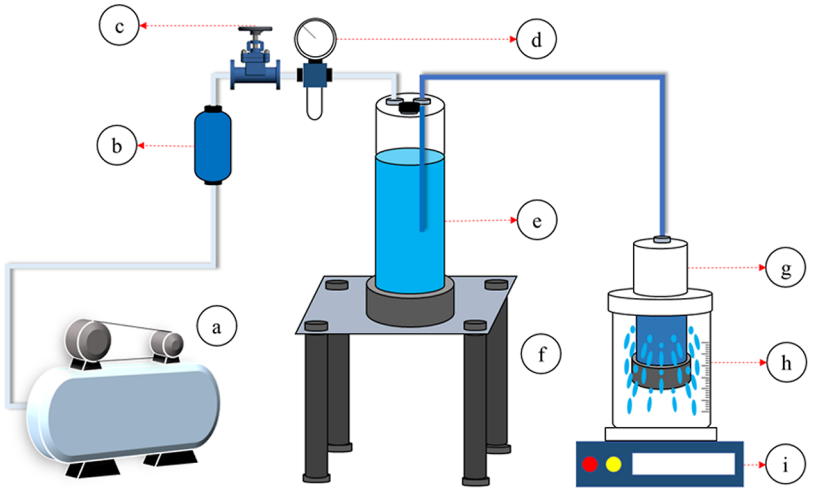

Figure 2. Schematic diagram of the cross-flow membrane flux apparatus: (a) compressor, (b) air filter, (c) valve, (d) pressure indicator, (e) water tank, (f) tank stand, (g) membrane holder, (h) membrane, and (i) mass balance.

https://doi.org/10.1021/acsomega.3c08379
ACS Omega 2024, 9, 11484−11493

following formula, taking into account parameters such as the volume of the permeate (V), membrane surface area (A), and filtration time (t).

$$J = \frac{V}{t \cdot A} \quad (1)$$

Here, V represents the volume of permeate Liters (L), A denotes the membrane surface area in square meters (m^2), and t signifies the duration of the filtration process in hours (h).

3. RESULTS AND DISCUSSION

3.1. Elemental Analysis of Foulants. Prior to the treatment, we characterized the elemental analysis of a dye serving as a foulant agent using XRF as depicted in Figure 3a.

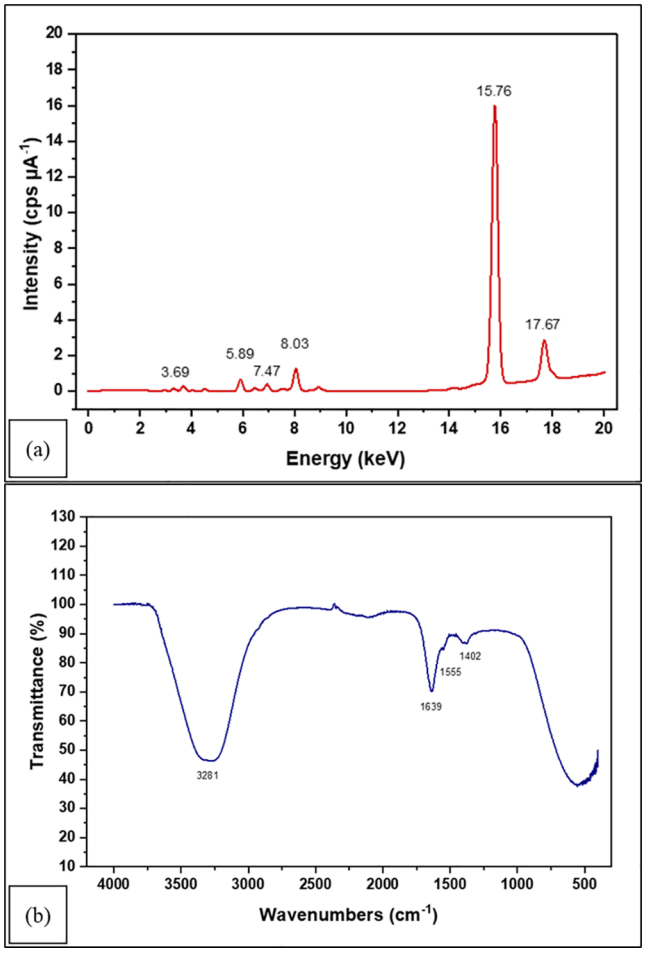

Figure 3. (a) XRF pattern of a dye as a foulant in the membrane and (b) FTIR spectrum of a dye as a foulant in the membrane.

XRF analysis of the foulant unveils the presence of elemental constituents, namely, calcium (Ca), manganese (Mn), nickel (Ni), copper (Cu), and zirconium (Zr). The identification of these elements was accomplished through the detection of their characteristic peaks during the analysis. Specifically, the following elemental peaks were observed:[34,35] Ca exhibited a peak at 3.690 keV, designated as Ca-Kα; Mn displayed a peak at 5.896 keV, referred to as Mn-Kα; Ni exhibited a characteristic peak at 7.476 keV, denoted as Ni-Kα; Cu manifested as a peak at 8.046 keV, identified as Cu-Kα; lastly, Zr showed a distinctive peak at 15.771 keV, known as Zr-Kα.

Furthermore, the FTIR analysis provides vibrational detailed inputs into the functional group of foulants, as depicted in Figure 3b. The presence of a peak at 3281 cm^{-1} indicates the hydrogen bond that is usually found in the range between 3650 and 3250 cm^{-1}. Another significant feature in the FTIR is the peak at 1639 cm^{-1}. This peak is associated with the stretching vibration of the carbon−carbon double bonds (C═C). The presence of this peak implies the existence of unsaturated carbon compounds. Additionally, the foulant's FTIR spectrum displays peaks at 1555 and 1402 cm^{-1}. The peak at 1555 cm^{-1} corresponds to the stretching vibration of nitrogen−oxygen bonds, characteristic of aromatic compounds. Meanwhile, the peak at 1402 cm^{-1} is indicative of the stretching vibration of sulfur−oxygen bonds, specifically organic sulfates.[36]

3.2. Elemental Analysis of Membrane Surfaces. Figure 4a,b depict SEM images of the surface of fouled and clean membranes. The morphology observed initially reveals the presence of dark regions, which is attributed to the presence of pores, while the white areas could be associated with the membrane material and the foulant. Furthermore, the elemental composition is carried out using EDX analysis to provide detailed weight percentage information.

Further investigation using EDS revealed that these structures share a similar chemical composition to the contributing elements that were previously identified by XRF analysis, as shown in Table 2. Notably, aside from titanium (Ti) and aluminum (Al) present in the membrane material itself, certain elements, namely, Zr, Mn, Ca, and Ni, exhibited a strong association with the foulant. Additionally, silicon (Si), a common microelement in water, particularly in groundwater, was also detected in this analysis.[37−39] Furthermore, the crucial constituents that are responsible for fouling are successfully demonstrated via subsequent reduction in the cleaning procedure, thereby indicating the successful efficacy of the cleaning process in mitigating foulant accumulation. Alongside the decrease in the weight percentages of foulants, the membrane components also exhibited an augmentation. Additionally, employing the surface porosity method by Abdullah and Khairurrijal,[31] the result revealed that the fouled membrane exhibited a lower surface porosity (59.9%) compared to its cleaned state (63.5%). It is readily apparent that fouling could lead to a decrease in porosity. This is because fouling can block the pores in the membrane, preventing water from flowing through this membrane.[40,41] However, the fouling was successfully removed from the membrane pores, facilitating incremental changes of the membrane porosity.

Furthermore, the cross-sectional morphology of the membrane was also examined, as depicted in Figure 4c,d. It is evident that there was a reduction in the deposited foulant in the outer edge region of the membrane, which corresponds to the entry point for the dye solution. Initially, the thickness of the deposited foulant was estimated to be 16 μm, while the cleaned membrane exhibited a thickness of only 13 μm. The oxidation process in this region effectively reduced the presence of the deposited foulant. EDX analysis results of the fouled membrane in the cross-sectional area are illustrated in Table 3. Notably, sodium (Na) could be detected in this analysis, likely attributed to the foulant. Na has a relatively low atomic number (11), which means that the X-rays emitted by Na possess a low emission energy. This makes it difficult to separate the Na signal from the background noise.[42] Thus, it is challenging to detect this element solely by using XRF.

https://doi.org/10.1021/acsomega.3c08379
ACS Omega 2024, 9, 11484−11493

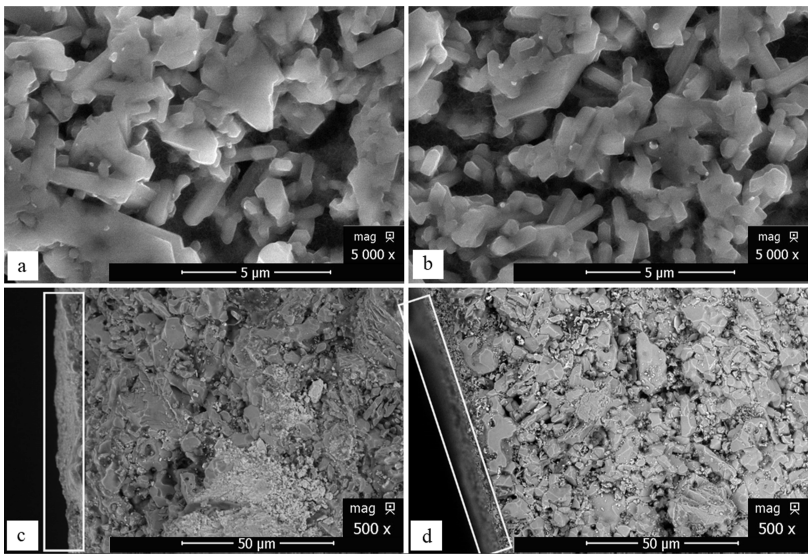

Figure 4. SEM images of the (a) fouled membrane surface and (b) cleaned membrane surfaces and the cross-sectional area of the (c) fouled membrane and the (d) cleaned membrane.

Table 2. EDX Analysis of the Surface Area of the Fouled Membrane and Cleaned Membrane

condition	weight (%)						
	Ti	Al	Si	Zr	Mn	Ca	Ni
fouled	95.7	1.8	1.0	0.6	0.5	0.3	0.1
cleaned	96.6	2.0	0.6	0.3	0.3	0.2	0.0

Additionally, the other elements of the foulant, namely, Ca, Cu, and Ni, were also quantifiable in this cross-sectional area. After the cleaning process, most of these elements exhibited a decrease in their weight percentage. Na and Ca, initially present at 0.50 and 0.35%, respectively, were reduced to 0.38 and 0.29%. Similarly, the weight percentages of Cu, Ni, and Mn decreased from 0.08, 0.01, and 0.30% to 0%. However, Zr elements could not be detected in this particular cross-sectional area. Conversely, the membrane elements, Ti, Al, and O, exhibited an increase in their weight and atomic proportions due to the reduction in the other elements. The proportion of carbon (C) associated with the organic components that are present in the dye solution has shown substantial changes, indicating that the oxidation process disrupted the chemical bonds among the organic components. Meanwhile, the presence of oxygen can be attributed to the membrane element and the organic constituents of the foulant. In XRF analysis, the identification of both C and O were challenging due to the low energy fluorescence exhibited by these elements.[43,44] Finally, the appearance of the chlorine element observed in the EDX analysis data can be linked to the utilization of process water, which is used for diluting the dye within the factory.

3.3. Analysis of Surface Morphologies. The three-dimensional morphological characteristics of both the fouled and cleaned membrane surfaces were further examined by using AFM shown in Figure 5. These analyses provided insights into the surface topography of the membrane. Prior to cleaning, the membrane surface exhibited a smoother appearance, as indicated by the root-mean-square (rms) roughness value of ∼93.65 nm. In contrast, the cleaned membrane displayed a rough and undulating surface, with an rms roughness of ∼109.6 nm. The variation in the surface roughness between the fouled and cleaned states offers valuable information regarding the deposition of foulants on the membrane surface.

It is important to note that contaminants have the ability to mask the inherent undulations of the membrane surface, resulting in a seemingly smoother surface after their deposition. The degree of surface roughness can influence the fouling rate in some ways. Rougher surfaces can provide more surface area for contaminants to attach to as well as increase the friction between the membrane and the fluid.[12,45,46] Consequently, this phenomenon impedes the upward movement of contaminants from the membrane surface and promotes their accumulation. Following the cleaning process, the roughness of the membrane surface increased, which can be attributed to the reduction in foulants that covered the initially rough surface.

3.4. Cleaning Mechanism. Figure 6 sheds light on how the ROS is generated from the ozone-NBs and how the subsequent cleaning process occurs in ceramic membranes. Three sequential paths were proposed in the cleaning process including ROS generation from the oxidative agent, continued by foulant encapsulation and foulant degradation. The oxidative agent was modified using a hydrodynamic cavitation process taking place in the NB generator. Initially, the pressurized ozone was injected into the water flow, following

Table 3. EDX Data of the Cross-Sectional Area of the Fouled Membrane and Defouled Membrane

condition	weight (%)											
	O	C	Al	Ti	Si	Na	Ca	Cu	Ni	Mn	Zr	Cl
fouled	46.03	25.56	15.24	10.79	0.97	0.50	0.35	0.08	0.01	0.30	0.00	0.17
defouled	51.00	16.79	18.49	13.73	1.04	0.38	0.29	0.00	0.00	0.00	0.00	0.08

https://doi.org/10.1021/acsomega.3c08379
ACS Omega 2024, 9, 11484−11493

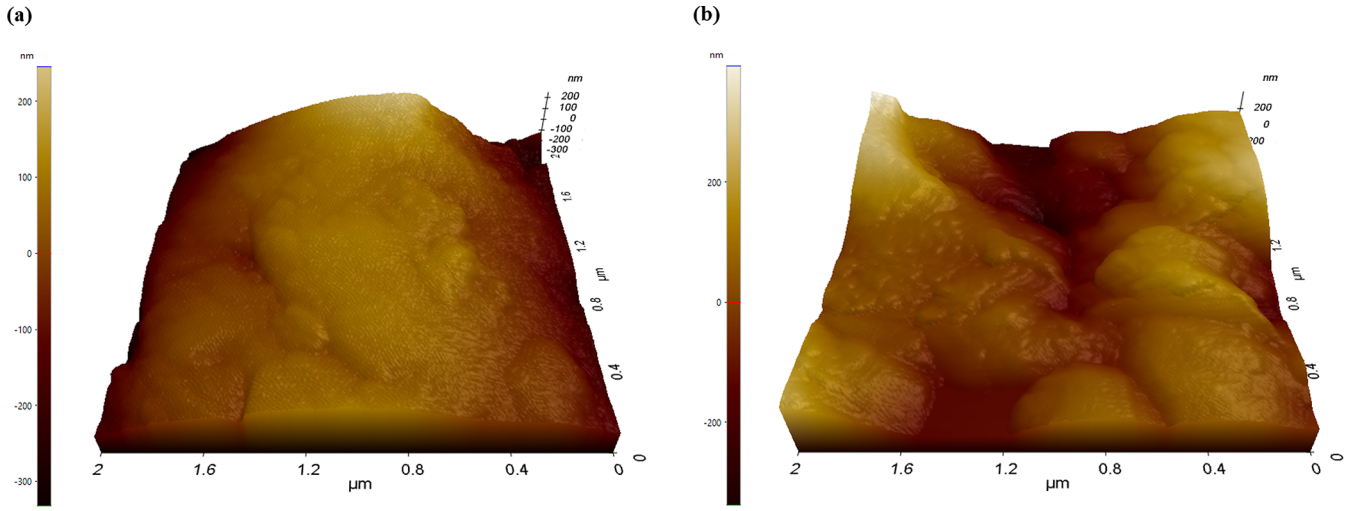

Figure 5. Three-dimensional topographic AFM images of the membrane surface: (a) fouled membrane and (b) cleaned membrane.

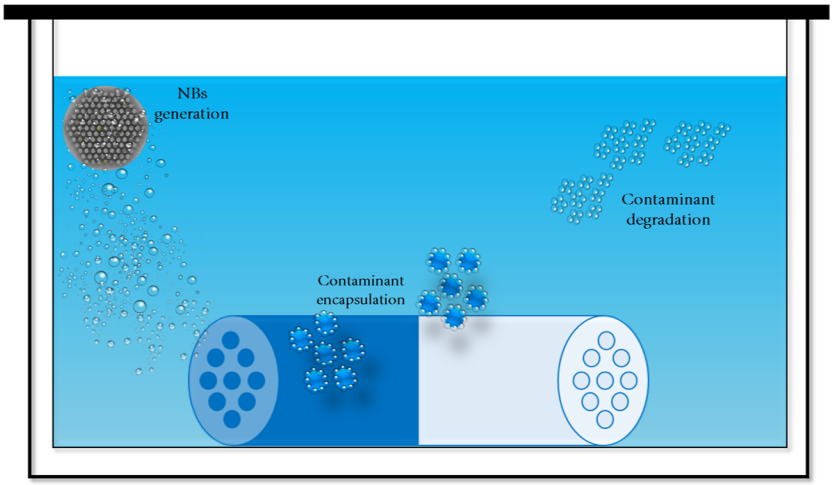

Figure 6. Proposed mechanisms of the ceramic membrane cleaning process.

the methodology described in the previous studies.[17,27,47] The multiphase flow, consisting of ozone and water, passed through the honeycomb structure of the NB generator. As the multiphase flow traversed the honeycomb structure, the breakdown of the flow led to the subsequent formation of ozone NBs. The product ozone NB has a higher surface contact compared to the MBs.

The physical modification significantly influences the further process of ROS generation.[9−50] We rationalize that the conventional thermodynamics of the bubble collapse phenomenon led to ozone breakdown. Furthermore, this process comprises three sequential stages, namely, initiation, propagation, and termination. The following Young−Laplace equation provided an explanation on the stability and behavior of the gas−liquid interface within the NBs.[51,52]

$$\Delta P = 2\gamma/R \tag{2}$$

ΔP is the pressure difference across the curved interface, γ is the surface tension of the liquid−gas interface, and R is the radius of curvature of the interface. When an NB forms, it exhibits a curved interface due to the surface tension of the liquid. The pressure inside the bubble is greater than the pressure outside, resulting in a pressure difference across the curved interface. This pressure difference can be described using Young−Laplace eq 2, which states that it is inversely proportional to the radius of curvature of the interface. In simpler terms, smaller bubbles with smaller radii of curvature will experience higher pressure differences across their interfaces compared to larger bubbles.[51−53] Consequently, the pressure inside the NBs can be significantly higher than the surrounding pressure. This pressure difference contributes to the structural stability of NBs, preventing their rapid dissolution. The elevated internal pressure helps to counterbalance the tendency of the bubble to shrink and maintain its integrity over an extended period. This increased pressure within the NB is crucial for sustaining its existence and prolonging its lifetime. The collapse of NBs results in the generation of highly localized pressures and temperatures, known as cavitation.[54] The high temperatures and pressures experienced during collapse lead to the formation of ROS specifically hydroxyl radicals ($^{\bullet}$OH).[55−57] Due to their high reactivity, hydroxyl radicals rapidly react with a broad range of organic contaminants, including pollutants, pathogens, and dyes.[17,58,59]

Figure 7a,b represents the size and zeta potential of NBs upon 4 h processing, respectively. The peak distribution value, representing 100% of the ozone-NB, is found to be ∼213.2 nm in size. Notably, the quantity and size of NBs can significantly

https://doi.org/10.1021/acsomega.3c08379
ACS Omega 2024, 9, 11484−11493

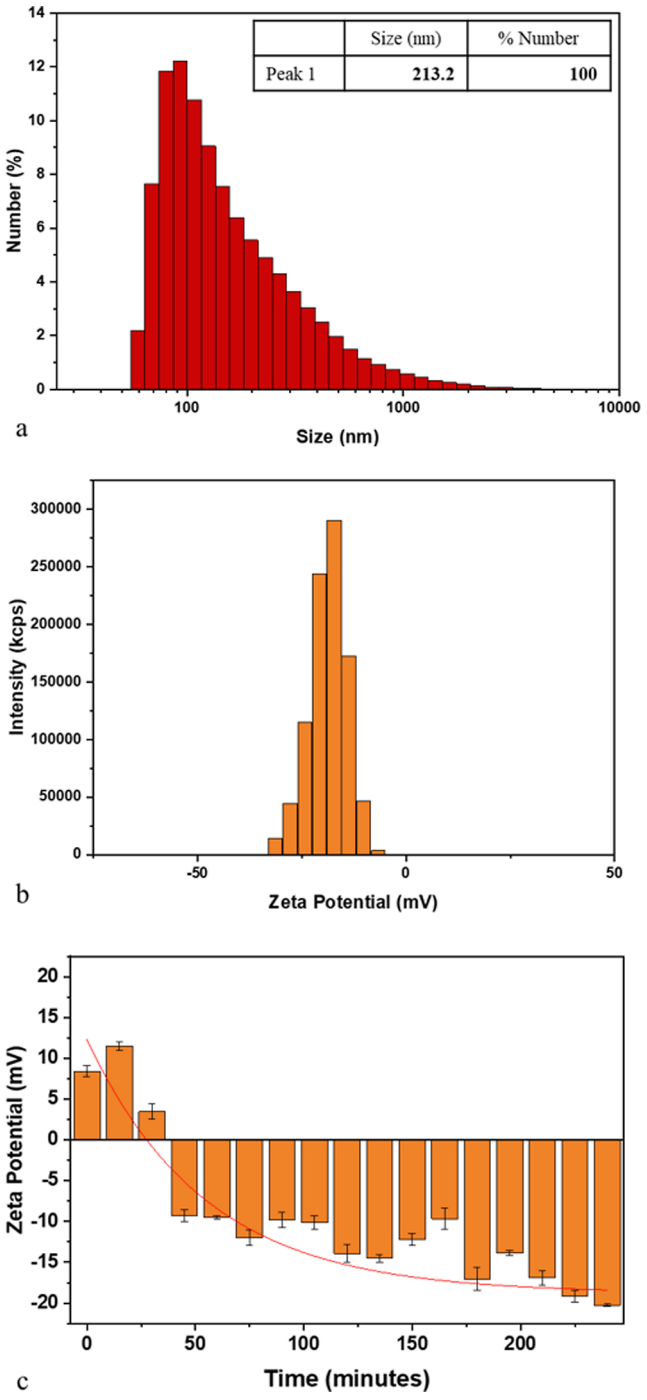

Figure 7. (a) Particle size distribution of ozone-NBs with the *x*-axis is plotted in the logarithmic scale. (b) Zeta potential value of ozone-NBs after a 4 h process. (c) Dynamic changes in zeta potential over the sequential 4 h process.

impact their mass transfer efficiency. We propose that producing a substantial amount of the desired NBs with a large surface area would enhance the mass transfer flow in the cleaning process.

The zeta potential of the NBs was measured at about −20.26 ± 0.13 mV at the final residence time of 240 min. The corresponding distribution of the zeta potential is shown in Figure 7b. Upon examining the evolution of zeta potential from the beginning to the 240 min markedly the turnover process that evidently led the zeta value transition from a positive to increasingly negative value, signaling the introduction of ROS into the targeted solution. Figure 7c and Table S1 exhibit the alteration of zeta potential throughout the sequential 4 h process.

The zeta potential of NBs plays a significant role in determining their stability and behavior within the colloidal system.[60,61] Various factors can influence the zeta potential of NBs, including the surface charge and composition of the surrounding liquid medium.[54,62] In this case, the presence of ROS could impact the zeta potential of colloidal particles, including NBs. ROS interacts with the surface of particles, leading to surface charge variation that subsequently affects the zeta potential. The negative zeta potential observed here is attributed to the presence of the generated ROS at the bubble interface, which contributes to the stability of NBs.[7,21,63] It is important to note that the zeta potential primarily reflects the charge of the bubble rather than its density in water. The electrically charged surface of the NBs causes particles to repel one another, preventing coalescence or merging of bubbles. This electrostatic repulsion plays a crucial role in maintaining the stability of the NBs and preventing their aggregation or coagulation with other bubbles or particles in the surrounding medium.[63−65]

We systematically varied the cleaning time to examine the remediation recovery in four different durations: 1, 2, 3, and 4 h, while maintaining a fixed pressure of 3 bar. The ceramic membrane was evaluated in both its initial fouled state and upon the cleaning procedure and then compared with the pristine state. Figure 8 provides a visual representation of the alterations observed in the ceramic membrane during the cleaning process. Initially, the fouled part of the membrane is visible, appearing as a dark blue color, indicating the presence of deposited foulants in the membrane channels. As the cleaning process progresses, the color gradually becomes lighter and more homogeneous, indicating the removal of fouling materials. In the final stage, after the 4 h process, the membrane's appearance transforms into a light blue color, and no visible deposits can be found in the membrane channels. Compared to that in a pristine state, the 4 h state displayed a similar visual condition. This visual evidence confirms the effectiveness of the cleaning process in restoring the cleanliness of the ceramic membrane.

Moreover, the average membrane flux values obtained in the four different cleaning times are 662, 800, 932, and 1050 L/h/m^2 for 1, 2, 3, and 4 h, respectively. In comparison, the fouled state exhibited a membrane flux of 608 L/h/m^2 while the pristine water flux was 1500 L/h/m^2. Detailed information can be found in Figure 9 and Table S2.

Notably, over the 4 h cleaning process, the flux recovery reached 50% and its flux was nearly doubled compared to the fouled state. This observation suggests that the accumulation of ROS, as previously mentioned, played a crucial role in effectively reducing the foulant on the membrane surface.[3] The continuous generation and accumulation of ROS during the extended cleaning time likely contributed to the enhanced reduction of foulants, leading to an improved water permeability of the membrane. These results highlight the importance of prolonged cleaning cycles in achieving a higher membrane flux and overall improved performance of the ceramic membrane system.

https://doi.org/10.1021/acsomega.3c08379
ACS Omega 2024, 9, 11484−11493

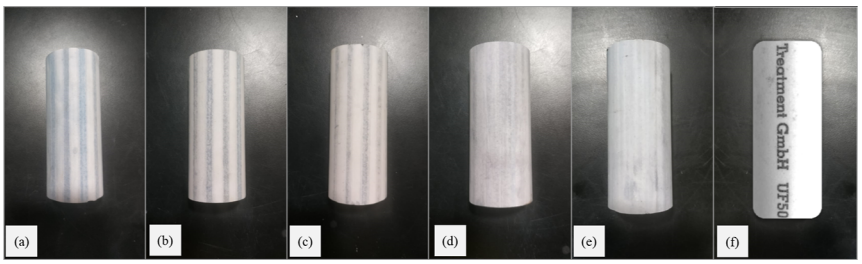

Figure 8. Visual progression of membrane conditions (a) before cleaning and after (b) 1, (c) 2, (d) 3, and (e) 4 h of the cleaning process compared to the (f) pristine state.

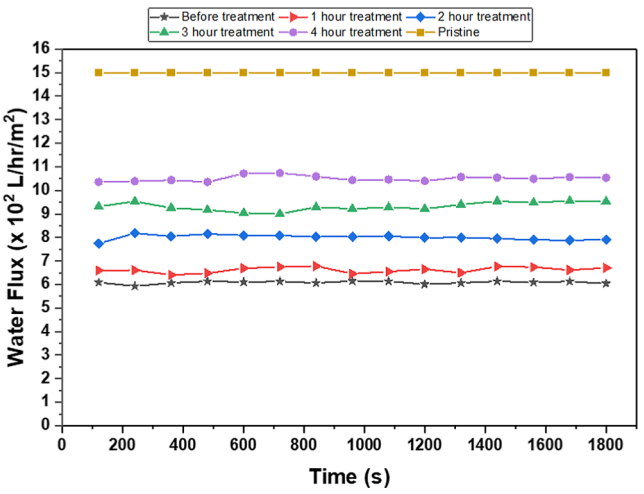

Figure 9. Membrane flux of the ceramic membranes in different treatment times: 0 h (black stars); 1 h (red triangles); 2 h (blue diamonds); 3 h (green triangles); and 4 h (purple circles) at a fixed pressure of 3 bar compared to the pristine state (yellow squares).

4. CONCLUSIONS

The study revealed a significant improvement in the remediation performance of the ceramic membrane upon the cleaning procedure by ozone-NBs, as evidenced by a remarkable increase in membrane flux from its initial value of 609 to 1051 L/h/m^2. The membrane underwent continuous changes over 4 h, transitioning from a dark blue color (indicating the presence of dye fouling) to a lighter shade of blue, indicating a reduction in dye fouling on the membrane surface. We propose findings originating from ROS generation during ozone-NB cavitation. This hypothesis is supported by the DLS analysis with the zeta potential resulting in a negative value (-20.26 ± 0.13 mV). This indicates the presence of predominantly negatively charged surfaces in the water associated with the characteristic feature of ROS. Furthermore, quantitative analysis revealed that 100% of the ozone-NBs with a size of 213.2 nm is observed in the water stream during the 4 h cleaning period. This finding further confirms the generation and presence of ozone-NBs, which are believed to contribute substantially to the efficient foulant removal from the ceramic membrane. Overall, this integrated ozone-NB system exhibits significant potential as an innovative and sustainable technology for effectively removing foulants in water treatment applications.

■ ASSOCIATED CONTENT

Supporting Information

The Supporting Information is available free of charge at https://pubs.acs.org/doi/10.1021/acsomega.3c08379.

Detailed data of zeta potential and membrane flux evolution during the sequential cleaning process (PDF)

■ AUTHOR INFORMATION

Corresponding Authors

Alfian Noviyanto − *Nano Center Indonesia, South Tangerang, Banten 15314, Indonesia; Department of Mechanical Engineering, Faculty of Engineering, Mercu Buana University, Kebun Jeruk, Jakarta 11650, Indonesia;* orcid.org/0000-0002-6371-6765; Email: a.noviyanto@nano.or.id, alfian.noviyanto@mercubuana.ac.id

Arramel − *Nano Center Indonesia, South Tangerang, Banten 15314, Indonesia;* orcid.org/0000-0003-4125-6099; Email: arramel@nano.or.id

Authors

Ande F. Rafryanto − *Nano Center Indonesia, South Tangerang, Banten 15314, Indonesia; Department of Chemical Engineering, Imperial College London, London SW72AZ, U.K.;* orcid.org/0000-0003-3542-6813

Zakia D. P. Ramadina − *Nano Center Indonesia, South Tangerang, Banten 15314, Indonesia*

Syarifa Nur'aini − *Nano Center Indonesia, South Tangerang, Banten 15314, Indonesia*

Bagas H. Arrosyid − *Nano Center Indonesia, South Tangerang, Banten 15314, Indonesia*

Akmal Zulfi − *Nano Center Indonesia, South Tangerang, Banten 15314, Indonesia; Research Center for Environmental and Clean Technology, National Research and Innovation Agency (BRIN), Bandung 40135, Indonesia;* orcid.org/0000-0003-4650-1399

Nurul T. Rochman − *Nano Center Indonesia, South Tangerang, Banten 15314, Indonesia; Research Center for Advanced Materials, National Research and Innovation Agency, South Tangerang, Banten 15314, Indonesia*

Complete contact information is available at: https://pubs.acs.org/10.1021/acsomega.3c08379

Author Contributions

Ande Fudja Rafryanto: Investigation, Formal analysis, and Writing-Original Draft; **Zakia Dwi Puspa Ramadina**: Project administration, Resources; **Syarifa Nur'aini**: Investigation; **Bagas Haqi Arrosyid**: Investigation; **Akmal Zulfi**: Conceptualization, Methodology, Supervision; **Nurul Taufiqu Rochman**: Funding acquisition, Supervision; **Alfian Noviyanto**:

https://doi.org/10.1021/acsomega.3c08379
ACS Omega 2024, 9, 11484−11493

Conceptualization, Validation, Writing-Review and Editing; **Arramel**: Validation, Supervision, Writing-Review and Editing.

Notes

The authors declare no competing financial interest.

■ ACKNOWLEDGMENTS

The authors would like to express their sincere gratitude to Nano Center Indonesia for their valuable support throughout this research. Additionally, the authors extend their appreciation to PT Nanotech Indonesia Global, Tbk. for providing the start-up research grant that contributed to the success of this study. The authors would also like to acknowledge the support received from Perusahaan Umum Percetakan Uang Republik Indonesia and PT NB Karya Indonesia.

■ REFERENCES

(1) Speed, D. E. Environmental Aspects of Planarization Processes. *Advances in Chemical Mechanical Planarization (CMP)*, 2016; pp 229−269.

(2) Meiramkulova, K.; Devrishov, D.; Zhumagulov, M.; Arystanova, S.; Karagoishin, Z.; Marzanova, S.; Kydyrbekova, A.; Mkilima, T.; Li, J. Performance of an Integrated Membrane Process with Electrochemical Pre-Treatment on Poultry Slaughterhouse Wastewater Purification. *Membranes* **2020**, *10* (10), 256.

(3) Ghadimkhani, A.; Zhang, W.; Marhaba, T. Ceramic Membrane Defouling (Cleaning) by Air Nano Bubbles. *Chemosphere* **2016**, *146*, 379−384.

(4) Davoodbeygi, Y.; Askari, M.; Salehi, E.; Kheirieh, S. A Review on Hybrid Membrane-Adsorption Systems for Intensified Water and Wastewater Treatment: Process Configurations, Separation Targets, and Materials Applied. *J. Environ. Manage.* **2023**, *335*, 117577.

(5) Fu, H.; Li, Z.; Zhang, Y.; Zhang, H.; Chen, H. Preparation, Characterization and Properties Study of a Superhydrophobic Ceramic Membrane Based on Fly Ash. *Ceram. Int.* **2022**, *48* (8), 11573−11587.

(6) Park, S. H.; Park, Y. G.; Lim, J. L.; Kim, S. Evaluation of Ceramic Membrane Applications for Water Treatment Plants with a Life Cycle Cost Analysis. *Desalin. Water Treat.* **2015**, *54* (4−5), 973−979.

(7) Zhou, S.; Marcelino, K. R.; Wongkiew, S.; Sun, L.; Guo, W.; Khanal, S. K.; Lu, H. Untapped Potential: Applying Microbubble and Nanobubble Technology in Water and Wastewater Treatment and Ecological Restoration. *ACS ES&T Engg* **2022**, *2* (9), 1558−1573.

(8) Gul, A.; Hruza, J.; Yalcinkaya, F. Fouling and Chemical Cleaning of Microfiltration Membranes: A Mini-Review. *Polymers* **2021**, *13* (6), 846.

(9) Doan, N. T. T.; Lai, Q. D. Ultrafiltration for Recovery of Rice Protein: Fouling Analysis and Technical Assessment. *Innovative Food Sci. Emerging Technol.* **2021**, *70*, 102692.

(10) Li, H.; Chen, V. Membrane Fouling and Cleaning in Food and Bioprocessing. *Membr. Technol.* **2010**, 213−254.

(11) Hilal, N.; Ogunbiyi, O. O.; Miles, N. J.; Nigmatullin, R. Methods Employed for Control of Fouling in MF and UF Membranes: A Comprehensive Review. *Sep. Sci. Technol.* **2005**, *40* (10), 1957−2005.

(12) Yin, N.; Zhong, Z.; Xing, W. Ceramic Membrane Fouling and Cleaning in Ultrafiltration of Desulfurization Wastewater. *Desalination* **2013**, *319*, 92−98.

(13) Guillen-Burrieza, E.; Ruiz-Aguirre, A.; Zaragoza, G.; Arafat, H. A. Membrane Fouling and Cleaning in Long Term Plant-Scale Membrane Distillation Operations. *J. Membr. Sci.* **2014**, *468*, 360−372.

(14) Dayarathne, H. N. P.; Choi, J.; Jang, A. Enhancement of Cleaning-in-Place (CIP) of a Reverse Osmosis Desalination Process with Air Micro-Nano Bubbles. *Desalination* **2017**, *422*, 1−4.

(15) Temesgen, T.; Bui, T. T.; Han, M.; Kim, T.; Park, H. Micro and Nanobubble Technologies as a New Horizon for Water-Treatment Techniques: A Review. *Adv. Colloid Interface Sci.* **2017**, *246*, 40−51.

(16) Naffrechoux, E.; Chanoux, S.; Petrier, C.; Suptil, J. Sonochemical and Photochemical Oxidation of Organic Matter. *Ultrason. Sonochem.* **2000**, *7* (4), 255−259.

(17) Hutagalung, S. S.; Rafryanto, A. F.; Sun, W.; Juliasih, N.; Aditia, S.; Jiang, J.; Arramel; Dipojono, H. K.; Suhardi, S. H.; Rochman, N. T.; Kurniadi, D. Combination of Ozone-Based Advanced Oxidation Process and Nanobubbles Generation toward Textile Wastewater Recovery. *Front. Environ. Sci.* **2023**, *11*, 1154739.

(18) Sotelo, J. L.; Beltran, F. J.; Benitez, F. J.; Beltran-heredia, J. Ozone Decomposition in Water: Kinetic Study. *Ind. Eng. Chem. Res.* **1987**, *26* (1), 39−43.

(19) Inoue, S.; Kimura, Y.; Uematsu, Y. Ostwald Ripening of Aqueous Microbubble Solutions. *J. Chem. Phys.* **2022**, *157* (24), 244704.

(20) Pan, Y.; He, B.; Wen, B. Effects of Surface Tension on the Stability of Surface Nanobubbles. *Front. Phys.* **2021**, *9*, 731804.

(21) Selihin, N. M.; Tay, M. G. A Review on Future Wastewater Treatment Technologies: Micro-Nanobubbles, Hybrid Electro-Fenton Processes, Photocatalytic Fuel Cells, and Microbial Fuel Cells. *Water Sci. Technol.* **2022**, *85* (1), 319−341.

(22) Suvira, M.; Zhang, B. Effect of Surfactant on Electrochemically Generated Surface Nanobubbles. *Anal. Chem.* **2021**, *93* (12), 5170−5176.

(23) Hu, L.; Xia, Z. Application of Ozone Micro-Nano-Bubbles to Groundwater Remediation. *J. Hazard. Mater.* **2018**, *342*, 446−453.

(24) Meegoda, J.; Batagoda, J. *A New Technology to Decontaminate Sediments Using Ultrasound with Ozone Nano Bubbles*; American Society of Civil Engineers, 2016.

(25) Tian, J. Y.; Xu, Y. P.; Chen, Z. L.; Nan, J.; Li, G. B. Air Bubbling for Alleviating Membrane Fouling of Immersed Hollow-Fiber Membrane for Ultrafiltration of River Water. *Desalination* **2010**, *260* (1−3), 225−230.

(26) Muhamad, M. S.; Salim, M. R.; Lau, W. J.; Yusop, Z.; Hadibarata, T. The Removal of Bisphenol A in Water Treatment Plant Using Ultrafiltration Membrane System. *Water, Air, Soil Pollut.* **2016**, *227* (7), 250.

(27) Rahmawati, A.; Saputra, R.; Hidayatullah, A.; Dwiarto, A.; Junaedi, H.; Cahyadi, D.; Saputra, H.; Prabowo, W.; Kartamiharja, U.; Shafira, H.; Noviyanto, A.; Rochman, N. Enhancement of Penaeus Vannamei Shrimp Growth Using Nanobubble in Indoor Raceway Pond. *Aquacult. Fish.* **2021**, *6*, 277−282.

(28) Saharan, V. K.; Rizwani, M. A.; Malani, A. A.; Pandit, A. B. Effect of Geometry of Hydrodynamically Cavitating Device on Degradation of Orange-G. *Ultrason. Sonochem.* **2013**, *20* (1), 345−353.

(29) Montalvo Andia, J. P.; Ticona Cayte, A. E.; Illachura Rodriguez, J. M.; López Belón, L.; Cárdenas Málaga, M. A.; Teixeira, L. A. C. Combined Treatment Based on Synergism between Hydrodynamic Cavitation and H2O2 for Degradation of Cyanide in Effluents. *Miner. Eng.* **2021**, *171*, 107119.

(30) Wang, J.; Chen, H.; Yuan, R.; Wang, F.; Ma, F.; Zhou, B. Intensified Degradation of Textile Wastewater Using a Novel Treatment of Hydrodynamic Cavitation with the Combination of Ozone. *J. Environ. Chem. Eng.* **2020**, *8* (4), 103959.

(31) Abdullah, M.; Khairurrijal, K. A Simple Method for Determining Surface Porosity Based on SEM Images Using OriginPro Software. *Indones. J. Sci. Technol.* **2016**, *20* (2), 37−40.

(32) Nur'aini, S.; Zulfi, A.; Arrosyid, B. H.; Rafryanto, A. F.; Noviyanto, A.; Hapidin, D. A.; Feriyanto, D.; Saputro, K. E.; Khairurrijal, K.; Rochman, N. T. Waste Acrylonitrile Butadiene Styrene (ABS) Incorporated with Polyvinylpyrrolidone (PVP) for Potential Water Filtration Membrane. *RSC Adv.* **2022**, *12* (52), 33751−33760.

(33) Abdelrazeq, H.; Khraisheh, M.; Hassan, M. K. Long-Term Treatment of Highly Saline Brine in a Direct Contact Membrane Distillation (DCMD) Pilot Unit Using Polyethylene Membranes. *Membranes* **2022**, *12* (4), 424.

https://doi.org/10.1021/acsomega.3c08379
ACS Omega 2024, 9, 11484−11493

(34) Pashkova, G.; Chubarov, V.; Akhmetzhanov, T.; Zhilicheva, A.; Mukhamedova, M.; Finkel'shtein, A.; Belozerova, O. Total-Reflection X-Ray Fluorescence Spectrometry as a Tool for the Direct Elemental Analysis of Ores: Application to Iron, Manganese, Ferromanganese, Nickel-Copper Sulfide Ores and Ferromanganese Nodules. *Spectrochim. Acta, Part B* **2020**, *168*, 105856.
(35) Purwadi, I.; Casey, L.; Ryan, C.; Erskine, P.; van der Ent, A. X-ray Fluorescence Spectroscopy (XRF) for Metallome Analysis of Herbarium Specimens. *Plant Methods* **2022**, *18*, 139.
(36) Nandiyanto, A. B. D.; Oktiani, R.; Ragadhita, R. How to Read and Interpret FTIR Spectroscope of Organic Material. *Indones. J. Sci. Technol.* **2019**, *4* (1), 97−118.
(37) Keesari, T.; Roy, A.; Pant, D.; Sinha, U. K.; Kumar, P. V. N.; Rao, L. V. Major Ion, Trace Metal and Environmental Isotope Characterization of Groundwater in Selected Parts of Uddanam Coastal Region, Andhra Pradesh, India. *J. Earth Syst. Sci.* **2020**, *129* (1), 205.
(38) Khan, A.; Umar, R.; Khan, H. H. Significance of Silica in Identifying the Processes Affecting Groundwater Chemistry in Parts of Kali Watershed, Central Ganga Plain, India. *Appl. Water Sci.* **2015**, *5* (1), 65−72.
(39) Turner, C.; Donose, B. C.; Kezia; Birkett, G.; Pratt, S. Silica Fouling during Groundwater RO Treatment: The Effect of Colloids' Radius of Curvature on Dissolution and Polymerisation. *Water Res.* **2020**, *168*, 115135.
(40) Sanaei, P.; Cummings, L. J. Flow and Fouling in Membrane Filters: Effects of Membrane Morphology. *J. Fluid Mech.* **2017**, *818*, 744−771.
(41) Virtanen, T.; Rudolph, G.; Lopatina, A.; Al-Rudainy, B.; Schagerlöf, H.; Puro, L.; Kallioinen, M.; Lipnizki, F. Analysis of Membrane Fouling by Brunauer-Emmett-Teller Nitrogen Adsorption/Desorption Technique. *Sci. Rep.* **2020**, *10* (1), 3427.
(42) Chen, H.; Rogalski, M. M.; Anker, J. N. Advances in Functional X-Ray Imaging Techniques and Contrast Agents. *Phys. Chem. Chem. Phys.* **2012**, *14* (39), 13469−13486.
(43) Otaka, A.; Hokura, A.; Nakai, I. Determination of Trace Elements in Soybean by X-Ray Fluorescence Analysis and Its Application to Identification of Their Production Areas. *Food Chem.* **2014**, *147*, 318−326.
(44) Ravansari, R.; Wilson, S. C.; Tighe, M. Portable X-Ray Fluorescence for Environmental Assessment of Soils: Not Just a Point and Shoot Method. *Environ. Int.* **2020**, *134*, 105250.
(45) Guo, J.; Zhang, Y.; Chen, F.; Chai, Y. A Membrane with Strong Resistance to Organic and Biological Fouling Using Graphene Oxide and D-Tyrosine as Modifiers. *Membranes* **2022**, *12* (5), 486.
(46) Li, W.; Ling, G.; Lei, F.; Li, N.; Peng, W.; Li, K.; Lu, H.; Hang, F.; Zhang, Y. Ceramic Membrane Fouling and Cleaning during Ultrafiltration of Limed Sugarcane Juice. *Sep. Purif. Technol.* **2018**, *190*, 9−24.
(47) Levitsky, I.; Tavor, D.; Gitis, V. Generation of Two-Phase Air-Water Flow with Fine Microbubbles. *Chem. Eng. Technol.* **2016**, *39* (8), 1537−1544.
(48) Liu, Y.; Wang, S.; Shi, L.; Lu, W.; Li, P. Enhanced Degradation of Atrazine by Microbubble Ozonation. *Environ. Sci.* **2020**, *6* (6), 1681−1687.
(49) Ogata, S.; Murata, Y. Disinfection of Escherichia Coli by Mixing with Bulk Ultrafine Bubble Solutions. *Fluids* **2022**, *7* (12), 383.
(50) Yu, X.; Wang, Z.; Lv, Y.; Wang, S.; Zheng, S.; Du, H.; Zhang, Y. Effect of Microbubble Diameter, Alkaline Concentration and Temperature on Reactive Oxygen Species Concentration. *J. Chem. Technol. Biotechnol.* **2017**, *92* (7), 1738−1745.
(51) Xue, S.; Zhang, Y.; Marhaba, T.; Zhang, W. Aeration and Dissolution Behavior of Oxygen Nanobubbles in Water. *J. Colloid Interface Sci.* **2022**, *609*, 584−591.
(52) Yildirim, T.; Yaparatne, S.; Graf, J.; Garcia-Segura, S.; Apul, O. Electrostatic Forces and Higher Order Curvature Terms of Young-Laplace Equation on Nanobubble Stability in Water. *NPJ Clean Water* **2022**, *5* (1), 18.
(53) Sakr, M.; Mohamed, M. M.; Maraqa, M. A.; Hamouda, M. A.; Aly Hassan, A.; Ali, J.; Jung, J. A Critical Review of the Recent Developments in Micro-Nano Bubbles Applications for Domestic and Industrial Wastewater Treatment. *Alexandria Eng. J.* **2022**, *61* (8), 6591−6612.
(54) Foudas, A. W.; Kosheleva, R. I.; Favvas, E. P.; Kostoglou, M.; Mitropoulos, A. C.; Kyzas, G. Z. Fundamentals and Applications of Nanobubbles: A Review. *Chem. Eng. Res. Des.* **2023**, *189*, 64−86.
(55) Soyluoglu, M.; Kim, D.; Zaker, Y.; Karanfil, T. Stability of Oxygen Nanobubbles under Freshwater Conditions. *Water Res.* **2021**, *206*, 117749.
(56) Liu, S.; Oshita, S.; Kawabata, S.; Makino, Y.; Yoshimoto, T. Identification of ROS Produced by Nanobubbles and Their Positive and Negative Effects on Vegetable Seed Germination. *Langmuir* **2016**, *32* (43), 11295−11302.
(57) Takahashi, M.; Shirai, Y.; Sugawa, S. Free-Radical Generation from Bulk Nanobubbles in Aqueous Electrolyte Solutions: ESR Spin-Trap Observation of Microbubble-Treated Water. *Langmuir* **2021**, *37* (16), 5005−5011.
(58) Vallejo, M.; Fresnedo San Román, M.; Ortiz, I.; Irabien, A. Overview of the PCDD/Fs Degradation Potential and Formation Risk in the Application of Advanced Oxidation Processes (AOPs) to Wastewater Treatment. *Chemosphere* **2015**, *118* (1), 44−56.
(59) Guo, X.-H.; Yang, Y.; Deng, Z.-Y. Filtrates with Hydroxyl Radicals Prepared Using Al + Acid + H2O2 for Removing Organic Pollutants. *ACS Omega* **2021**, *6* (22), 14182−14190.
(60) Calgaroto, S.; Wilberg, K. Q.; Rubio, J. On the Nanobubbles Interfacial Properties and Future Applications in Flotation. *Miner. Eng.* **2014**, *60*, 33−40.
(61) Wu, J.; Zhang, K.; Cen, C.; Wu, X.; Mao, R.; Zheng, Y. Role of Bulk Nanobubbles in Removing Organic Pollutants in Wastewater Treatment. *AMB Express* **2021**, *11* (1), 96.
(62) Kim, J. Y.; Song, M. G.; Kim, J. D. Zeta Potential of Nanobubbles Generated by Ultrasonication in Aqueous Alkyl Polyglycoside Solutions. *J. Colloid Interface Sci.* **2000**, *223* (2), 285−291.
(63) Ushikubo, F. Y.; Enari, M.; Furukawa, T.; Nakagawa, R.; Makino, Y.; Kawagoe, Y.; Oshita, S. Zeta-Potential of Micro- and/or Nano-Bubbles in Water Produced by Some Kinds of Gases. *IFAC Proc. Vol.* **2010**, *43* (26), 283−288.
(64) Meegoda, J. N.; Aluthgun Hewage, S.; Batagoda, J. H. Stability of Nanobubbles. *Environ. Eng. Sci.* **2018**, *35* (11), 1216−1227.
(65) Satpute, P. A.; Earthman, J. C. Hydroxyl Ion Stabilization of Bulk Nanobubbles Resulting from Microbubble Shrinkage. *J. Colloid Interface Sci.* **2021**, *584*, 449−455.

https://doi.org/10.1021/acsomega.3c08379
ACS Omega 2024, 9, 11484−11493